## APPLIED PHYSICS

# Generation and Diagnostics of Pulse Plasma Flows

**A. B. Tazhen[a],\*, Zh. R. Rayimkhanov[a],\*\*, M. K. Dosbolayev[a],\*\*\*, and T. S. Ramazanov[a],\*\*\*\***

[a] *Institute of Experimental and Theoretical Physics, al-Farabi Kazakh National University,*
*Almaty, 050040 Republic of Kazakhstan*
*\*e-mail: aigerim_tzh@mail.ru*
*\*\*e-mail: zhanikkaznu@gmail.com*
*\*\*\*e-mail: merlan@physics.kz*
*\*\*\*\*e-mail: ramazan@physics.kz*

**Abstract**—Pulsed plasma accelerators are widely used for the production of high-temperature pulsed plasma flows for fundamental and practical applications. The basic parameters of pulsed plasma accelerators are the characteristics of the external electric and magnetic circuits, as well as the structural and energy properties of the plasma flow. This work aims to characterize an IPU-30 pulsed plasma accelerator. The triple Langmuir probe method, calorimetric plasma energy density measurements, Rogowski coil, and high-speed visible imaging with a Phantom VEO710S fast camera are used to diagnose the pulsed plasma obtained in the IPU-30. The local plasma parameters such as electron temperature and density, the energy density of the pulsed plasma flow, pulsed plasma current, and also discharge current are experimentally obtained at different discharge voltages and air pressure in the chamber. The typical waveforms of the triple probe and Rogowski coil are presented in the form of oscillograms. The images of plasma formation in the discharge gap are obtained and the velocity of a pulsed plasma flow is measured.

## INTRODUCTION

Currently, pulsed plasma accelerators are widely used to obtain high-temperature and sufficiently dense plasma. Such devices have a number of features that make them more important, e.g., as sources of energy ions, thermonuclear neutrons, and hard X-ray radiation [1]. Therefore, pulsed plasma accelerators are effectively used in various fields: in thermonuclear power engineering to study the interaction of plasma with candidate materials of the first wall [2], in industry for surface modification (pulsed plasma deposition [3]), and also as various radiation sources, e.g., X-ray and ultraviolet radiation [4].

The interaction of powerful plasma flows and charged particles with wall materials during the operation of a tokamak leads to significant damage of the open surfaces, plasma instability, and pollution. The loss of the plasma's equilibrium and its breakdown on the wall are accompanied by the erosion of the material and the emission of dust particles containing tritium and the activated wall material [5]. Therefore, it becomes necessary to periodically replace the wall. The shutdown of the reactor reduces the established power utilization factor and harms the economic performance. Good assessments of the experimental works and the results of numerical simulations on the

formation and transportation of dust, as well as on the evaluation of the role of dust in modern thermonuclear facilities, are given in [6]. The scanning electron-force microscopy results indicate that dust particles extracted from the reactor volume have a spherical shape in some cases or are accumulated in the form of clusters formed of fine dust particles. The size of such particles varies from a few hundred nanometers to several tens of micrometers. Numerous similar studies are carried out to study the erosion of materials and the formation of dust in modern thermonuclear facilities [7–9]. Pulsed plasma accelerators are suitable experimental test benches providing a realistic environment for the simulation of processes occurring in the volume of modern tokamaks. A plasma accelerator is capable of producing plasma with an energy density of 100 to 500 J/cm$^2$. Such energy is achieved by a plasma flow at a speed of 10 to 10$^3$ km/s. The plasma parameters fully comply with the requirements expected in ITER.

Another field of application for pulsed plasma accelerators relates to plasma surface engineering. The method of the deposition of layers of fusible materials using pulsed plasma is called *pulsed plasma deposition* [10]. This method is effective, in particular, for fabricating various coatings. The advantages of pulsed
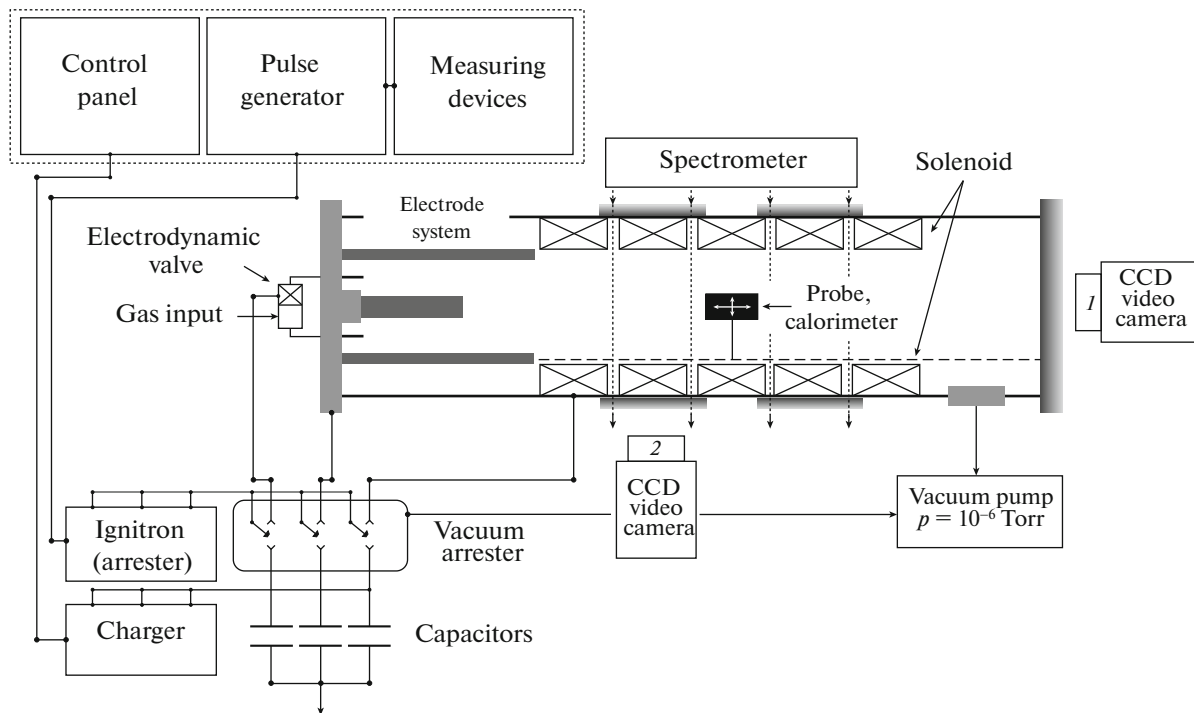
**Fig. 1.** Schematic diagram of a pulsed plasma accelerator.

methods are the increase in the internal energy of the thermodynamic system, achievement of a high plasma ionization degree during synthesis, and improvement in the morphology of the deposited films [11].

It should also be noted that, in comparison with a stationary plasma, the processes of energy exchange in a pulsed plasma occur for a short time. Thus, the synthesis products can cool rapidly on a dry substrate. It follows that the synthesis occurs inside the plasma itself. For example, aluminum nitride AlN layers were prepared in [3] by pulsed plasma deposition on a copper substrate. The pulsed plasma deposition method has not yet been fully studied; therefore, it is being studied extensively. For example, hard titanium nitride films that were prepared in [12] using this method. A pulsed plasma accelerator was used to fabricate semiconductor nanostructures from porous gallium arsenide (GaAs) [13]. The effect of the rapid thermal annealing on the indicated properties of porous nano-GaAs was studied.

Information on the main parameters of pulsed plasma is of great interest in the experimental simulation and studies of processes, in particular, the interaction of high-temperature plasma flows with the surface of the material. The main parameters of plasma accelerators are the characteristics of the external electric and magnetic circuits, as well as the structural and energy properties of the plasma flow. This work is devoted to a comprehensive diagnostics of the pulsed plasma flow in an IPU-30 experimental setup.

## EXPERIMENTAL SETUP

The IPU-30 experimental setup is a coaxial plasma accelerator [14, 15]. The accelerator is powered by capacitor banks with a total capacity of 1.44 mF. Plasma is formed and accelerated between two coaxial concentric electrodes, to which a high voltage is supplied through a switching device in the form of a vacuum arrestor. The diameter of the inner electrode is 55 mm, and that of the outer electrode is 108 mm. The plasma is accelerated to the output of the accelerator channel due to the longitudinal Ampere force, which occurs when the radial component of the volume current in the interelectrode space interacts with its own azimuthal magnetic field.

The lifetime of the plasma column in the coaxial accelerator channel is on the order of 300 μs. The accelerator's operating voltage is 3−6.5 kV. The facility was assembled at the Institute of Experimental and Theoretical Physics (Kazakhstan, Almaty) in the laboratory of dusty plasma and plasma technologies especially for the experimental simulation of the erosion of materials under the effect of the high-temperature pulsed plasma [16−18]. A schematic diagram of the IPU-30 coaxial accelerator is shown in Fig. 1.

## RESULTS AND DISCUSSION

The pulse plasma flow diagnostics includes a Langmuir triple electric probe, Rogowski coil, wire calorimeter, and high-speed shooting with a PhantomVEO710S camera. The Rogowski coil was used to
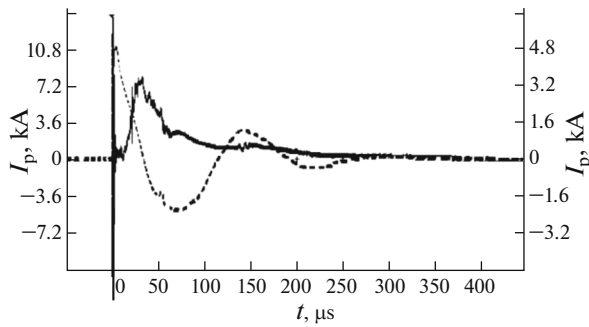
**Fig. 2.** Waveform of the signal from the Rogowski coil at the air pressure of 0.02 Torr: solid line is the plasma current and dotted line is the discharge current. The scale for the discharge current is indicated on the left and the scale for the plasma column current is indicated on the right.



**Fig. 3.** Dependence of the discharge current on the voltage on capacitors.

measure the discharge current and the plasma column's current at various voltage values on storage capacitors. The measuring toroidal coil consisted of 415 turns (a Rogowski coil with 94 turns was used to measure the plasma column current).

The ends of the turns were closed on a resistor with impedance of 1.3 Ω. The voltage drop on the resistance was measured on a LeCroy-354A digital storage oscilloscope. As an example, Fig. 2 shows the current waveform obtained in the IPU-30.

The signal detected by the belt is a damped sine wave. Based on such oscillograms, the maximum amplitude of the damped signal was used to plot the current−voltage (I−V) characteristic of the discharge at a fixed residual air pressure in the vacuum chamber of the accelerator at the level of 0.02 Torr (Fig. 3).

It can be seen (see Fig. 3) that the discharge current increases linearly with increasing voltage on the capacitors; i.e., Ohm's law is fulfilled, which indicates the absence of the current slip effect in this accelerator.

The results on the energy density of the pulsed plasma flow were obtained using a wire calorimeter [19] consisting of nichrome wires with a diameter of 340 μm stretched on a round fluoroplastic frame. The calorimeter was located at a distance of 15 cm from the end of the external accelerator electrode in the path of the plasma flow. The energy density of pulsed plasma is measured as follows: when the plasma flow passes through the wires they are heated and their resistance increases. With the knowledge of the change in the resistance of the wires, it is possible to calculate the amount of heat absorbed by the wires and, accordingly, the energy density.

In order to measure the change in the wire resistance, the calorimeter is connected to an electric circuit, which includes a measuring resistor $R_{sh}$ and a 1.5 V battery (see Fig. 4).

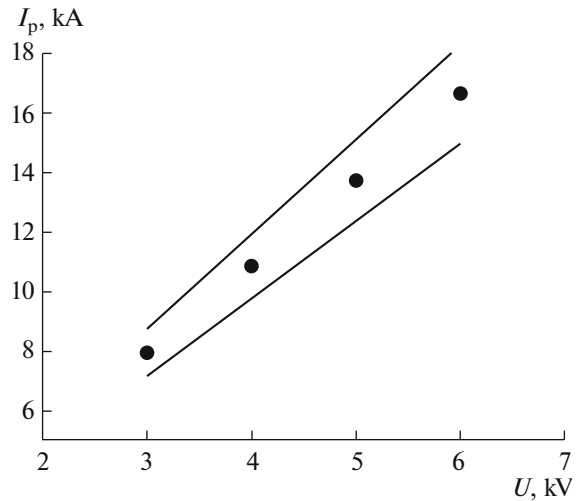The heating of wires is accompanied by the change in their resistivity, which can be written in the linear

approximation as $\rho = \rho_0 (1 + \alpha \Delta T)$. Here $\rho_0$ is the specific resistance of wires before heating, $\alpha$ is the temperature resistance coefficient, and $\Delta T$ indicates the change in temperature of the material after heating. Thus, knowing $\Delta T$, it is possible to find the amount of heat absorbed by the wires, and by the formula $Q = \int c\rho_m S \Delta T(l) dl$ ($\rho_m$ is the density of the material from which the wires are made) we obtain formula (1). Next, it is possible to calculate the energy density of the plasma flow:

$$\omega = \frac{c\rho_{nichrome}S^2}{\alpha\rho_0 S_{wire}}\Delta R, \qquad (1)$$

where $\omega$ is the plasma energy density, $c$ is the heat capacity of nichrome, $\rho_{nichrome}$ is the density of nichrome, $S$ is the cross section area of the nichrome
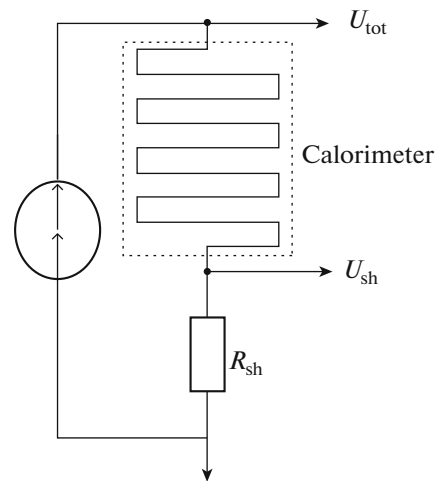


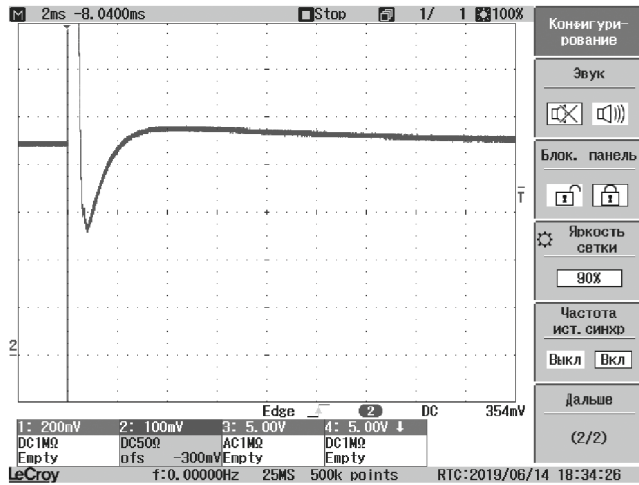**Fig. 4.** Electrical circuit for connecting the calorimeter.

**Fig. 5.** Voltage waveform on a measuring resistor at 3 kV. The scale on the waveform is set to 0.1 V/div and 2 ms/div.

wire, $\alpha$ is the temperature coefficient of the nichrome resistance, $\rho_0$ is the specific resistance of nichrome before heating, and $S_{wire}$ is the longitudinal cross section area of all the wires.

The energy density of the pulsed plasma flow was measured at two different storage capacitor voltages, namely, 3 and 4 kV. One of the signals on the measuring resistor obtained at 3 kV is shown in Fig. 5.

Based on the obtained waveforms and using formula (1), the plasma energy densities were calculated to be 175 J/cm$^2$ at the voltage on the capacitors of 3 kV and 328 J/cm$^2$ at the voltage on the capacitors of 4 kV. These results show that the plasma energy density increases with the increase in the voltage across the capacitors due to the increase in the kinetic energy of the plasma. Several regions can be distinguished on the waveform: at the beginning, when there is no plasma, the voltage across the measuring resistor remains constant over time; after the plasma is ignited (approximately 400 μs), a voltage jump in the calorimeter circuit appears in the oscillogram, which is due to the effect of charged plasma particles on the uninsulated wires (the time during which a strong voltage deviation is observed corresponds to the lifetime of the plasma bunch); after that, the voltage at the measuring resistor decreases, since after the plasma passes through the wires they heat up; i.e., the resistance of the wire calorimeter changes and this leads to a decrease in the voltage at the measuring resistor. The calculations take into account the voltage drop after the plasma exposure, which corresponds to the heating of the wires, and not to the voltage jump in the calorimeter circuit.

In the non-steady-state, the plasma media in which processes occur in very short time intervals, triple electric Langmuir probes are widely used to determine the local plasma parameters, such as the electron
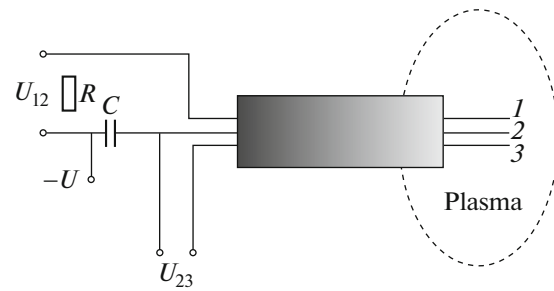
temperature and electron density [20]. The advantage of using triple electric probes in the IPU-30 pulsed plasma accelerator often lies in the fact that there is no need to plot the $I-V$ characteristics in contrast to conventional single and double probes. Using a triple probe, a direct measurement is carried out, i.e., without an additional voltage sweep. This method of determining the local plasma parameters is quite simple. The schematic diagram of a triple electric probe is shown in Fig. 6.



**Fig. 6.** Electric circuit for connecting a triple probe.

The triple probe consists of three graphite electrodes, each with a diameter of 0.5 mm. During the experiment, a triple probe was placed in the flow path, and the location of the triple probe was recorded through the side window of the accelerator (see Fig. 7). When the plasma reaches the tip of electrode *3*, the electrode begins to acquire the plasma potential (floating potential). Before the experiments, the other two electrodes *1* and *2* are shifted by a constant potential. The potential of one probe, to which electrons are attracted, is taken so that a current passes through it, equal in value but opposite in sign with respect to the probe, to which ions are attracted.

When electrode *3* acquires the plasma potential (negative or positive), which is also called the *floating potential*, there appears a difference in the potential between electrodes *2* and *3* equal in value to $U_{23}$. Using this potential difference, the electron temperature (in energy units) is determined by the following expression:

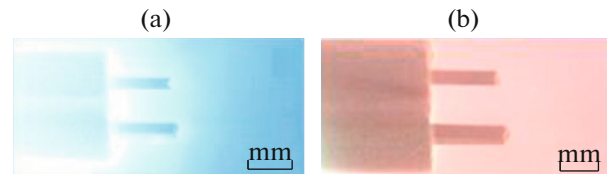$$kT_e = \frac{eU_{23}}{\ln 2}. \qquad (2)$$



**Fig. 7.** Triple electric probe placed in plasma: (a) a triple probe interacts with the tail of the plasma bunch, (b) after exposure. The acceleration of the plasma flow occurs from right to left.
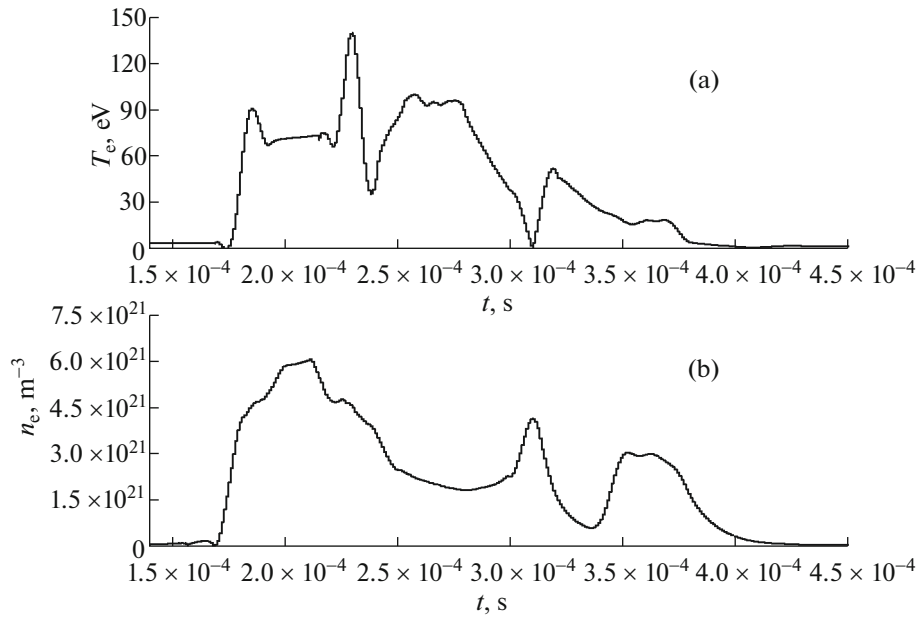
**Fig. 8.** Experimental data on electrons in the plasma flow in one shot: (a) electron temperature; (b) concentration.
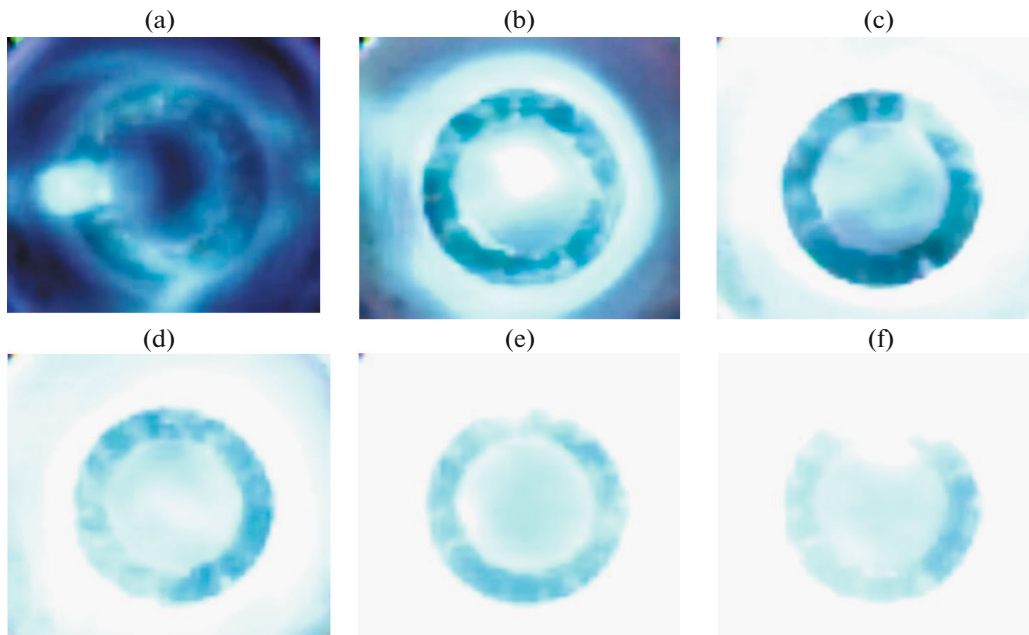


**Fig. 9.** Formation and development of the current (plasma) bridge of the gas discharge between the IPU electrodes (images obtained on the CCD camera in position *1*): (a) 3.5 μs; (b) 7 μs; (c) 10.5 μs; (d) 14 μs; (e) 17.5 μs; (f) 21 μs. The voltage at the electrodes is 4 kV. The outer contour of the black circle of 50 mm in the figures corresponds to the diameter of the inner electrode.

Using the known value of the electron temperature and based on formula (3), the electron concentration is determined:

$$n_e = \frac{-I}{0.61Ae\sqrt{\dfrac{kT_e}{m_i}}} \frac{\exp\left(-\dfrac{eU_{23}}{kT_e}\right)}{\left(1 - \exp\left(-\dfrac{eU_{23}}{kT_e}\right)\right)}, \qquad (3)$$

where $A$ is the electrode surface area, $m_i$ is the ion mass, $e$ is the electron charge, and $I$ is the ion saturation current. Since electrodes *1* and *2* have the same potential values but opposite signs the ion saturation current $I$ can be found through the potential difference between electrodes *1* and *2* of the triple probe.

The experiment was carried out at the air pressure of 0.02 Torr; therefore, the atomic mass of the nitrogen ion is taken into account in order to determine the
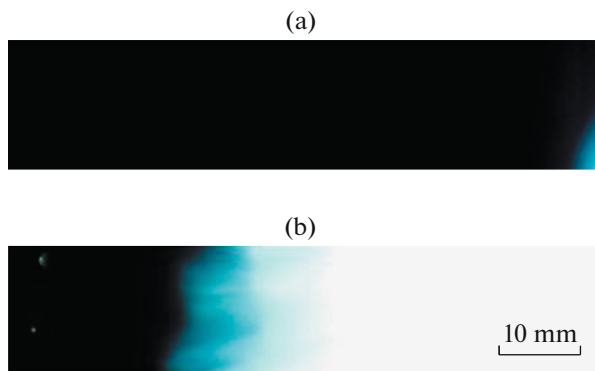
(a)



(b)



10 mm

**Fig. 10.** Instant photo of the accelerating plasma (images taken by a CCD camera in position *2*): (a) time of the plasma appearance; (b) formation of a plasma column and plasma acceleration. Frame rate of 510000 fps, exposure time of 1.5 μs, time between frames of 1.96 μs.

electron concentration. It was mentioned above that a triple electric probe allows direct measurements, which made it possible to obtain results on the electron temperature and their concentration in one "shot." Figure 8 shows the corresponding data in units of eV and $m^{-3}$.

Using a high-speed PhantomVEO710S camera, we calculated the velocity of a pulsed plasma flow and obtained the frames of the formation of a current (plasma) bridge of the gas discharge between the electrodes when applying a high voltage and accelerating the plasma along the vacuum chamber. The corresponding frames are shown in Figs. 9 and 10.

An instant pattern of the evolution of the filling of the interelectrode sectors with plasma, a strongly luminous ring-shaped region, was obtained (see Fig. 9b). Further, the plasma accelerates and moves beyond the interelectrode space (see Figs. 9c, 9f). The plasma lifetime in the interelectrode space is approximately 21 μs. During this time, the Ampere force acts on the plasma, and the plasma also is also heated strongly, which suffices to produce a large temperature gradient and, therefore, pressure (density). This leads to the appearance of an additional plasma acceleration force.

The acceleration of the plasma flow along the axis of the reactor was observed through the side window. Instant photographs of the accelerating plasma from the side were obtained (see Fig. 10).The plasma flow velocity of 26.6 km/s was determined from two plasma images, when the time and length of the path traveled were known.

## CONCLUSIONS

A pulsed plasma flow in an IPU-30 pulsed plasma accelerator was diagnosed using a triple electric probe, Rogowski coil, calorimeter, and a high-speed PhantomVEO710S camera. The electrical characteristics of the plasma column and discharge were obtained, and the energy density of the pulsed plasma was determined at different values of the voltage of the storage capacitor and air pressure. The local parameters of the pulsed plasma, such as the electron temperature and concentration in the flow, were determined using a Langmuir triple electric probe.

Instant photographs of the formation of a plasma bridge in the interelectrode space and plasma acceleration were obtained using a PhantomVEO710S high-speed camera. The velocity of the pulsed plasma flow of 26.6 km/s was determined from two frames.

## REFERENCES

1. H. Sadeghi, R. Amrollahi, M. Zare, and S. Fazel-pour, Plasma Phys. Controlled Fusion **59**, 125006 (2017).

2. A. Zhitlukhin, N. Klimov, I. Landman, J. Linke, A. Loarte, M. Merola, V. Podkovyrov, G. Federici, B. Bazylev, S. Pestchanyi, V. Safronov, T. Hirai, V. Maynashev, and V. Levashov, J. Nucl. Mater. **363–365**, 301 (2007).

3. K. Nowakowska-Langier, K. Zdunek, R. Chodun, S. Okrasa, R. Kwiatkowski, K. Malinowski, E. Skladnik-Sadowska, and M. Sadowski, Phys. Scr. **2014** (T161), 014063 (2014).

4. J. Jain, J. Moreno, R. Avila, G. Avaria, C. Pavez, B. Bora, S. Davis, and L. Soto, J. Phys.: Conf. Ser. **720**, 012048 (2018).

5. V. P. Smirnov, Ross. Khim. J. **6**, 79 (2008).

6. S. I. Krasheninnikov, R. D. Smirnov, and D. L. Rudakov, Plasma Phys. Controlled Fusion **53**, 083001 (2011).

7. E. Fortuna-Zaleśna, A. Weckmann, J. Grzonka, M. Rubel, H. G. Esser, M. Freisinger, A. Kreter, G. Sergienko, and P. Ström, Phys. Scr. **2016** (T167), 014059 (2016).

8. E. Fortuna-Zaleśna, J. Grzonka, M. Rubel, A. Garcia-Carrasco, A. Widdowson, A. Baron-Wiechec, L. Ciupiński, and JET Contributors, Nucl. Mater. Energy **12**, 582 (2017).

9. A. Autricque, S. H. Hong, N. Fedorczak, S. H. Son, H. Y. Lee, I. Song, W. Choe, and C. Grisolia, Nucl. Mater. Energy **12**, 599 (2017).

10. K. Zdunek, Surf. Coat. Technol. **201**, 4813 (2017).

11. K. Chodun, K. Nowakowska-Langier, and K. Zdunek, Mater. Sci.-Pol. **34** (3), 523 (2016).

12. S. Zeb, A. Qayyum, M. Shafiq, and M. Zakaullah, Eur. Phys. J.: Appl. Phys. **42**, 145 (2008).

13. O. Mangla, S. Roy, and K. Ostrikov, Nanomaterials **1**, 13 (2016).

14. M. Dosbolayev, Zh. Raiymkhanov, A. Tazhen, and T. Ramazanov, IEEE Trans. Plasma Sci. **7**, 3047 (2019).

15. A. Tazhen, A. Utegenov, M. Dosbolayev, T. Ramazanov, M. I. Kaikanov, and A. V. Tikhonov, Zh. Probl. Evol. Otkr. Syst. **18**, 40 (2016).

16. A. B. Tazhen, M. K. Dosbolayev, A. U. Utegenov, Zh. R. Raiymkhanov, and T. S. Ramazanov, in *XXIV Europhysics Conference on Atomic and Molecular Physics of Ionized Gases, Glasgow, 2018,* Book of Abstracts, p. 146.

17. M. K. Dosbolayev, A. U. Utegenov, A. B. Tazhen, T. S. Ramazanov, and M. T. Gabdullin, News Nat. Acad. Sci. Resp. Kazakhstan **310**, 59 (2016).

18. M. K. Dosbolayev, A. U. Utegenov, A. B. Tazhen, and T. S. Ramazanov, Laser and Part. Beams. **4**, 741 (2017).

19. A. V. Kireenko and S. V. Murakhtin, Vopr. At. Nauki Tekh., Ser.: Termoyad. Sint. **31** (1), 26 (2008).

20. S. Borthakur, N. Talukdar, N. K. Neog, and T. K. Borthakur, Fusion Eng. Des. **122**, 131 (2017).

*Translated by L.Mosina*